Near-threshold two-photon double ionization of Kr in the vacuum ultraviolet

Lazaros Varvarezos,[1] Stefan Düsterer,[2] Maksim D. Kiselev,[3,4,5] Rebecca Boll,[2,6] Cedric Bomme,[2,7] Alberto De Fanis,[6] Benjamin Erk,[2] Christopher Passow,[2] Sergei M. Burkov,[5] Gregor Hartmann,[2,8,9] Markus Ilchen,[9,6] Per Johnsson,[10] Thomas J. Kelly,[11] Bastian Manschwetus,[2] Tommaso Mazza,[6] Michael Meyer,[6] Dimitrios Rompotis,[6,2] Oleg Zatsarinny,[12] Elena V. Gryzlova,[3] Alexei N. Grum-Grzhimailo,[3] and John T. Costello[1]

[1]*School of Physical Sciences and National Centre for Plasma Science and Technology, Dublin City University, Dublin 9, Ireland*
[2]*Deutsches Elektronen-Synchrotron (DESY), Notkestrasse 85, D-22607 Hamburg, Germany*
[3]*Skobeltsyn Institute of Nuclear Physics, Lomonosov Moscow State University, Moscow 119991, Russia*
[4]*Lomonosov Moscow State University, Faculty of Physics, 119991 Moscow Russia*
[5]*Pacific National University, Tihookeanskaya Str., 139, Khabarovsk 680035, Russia*
[6]*European XFEL, Holzkoppel 4, 22869 Schenefeld, Germany*
[7]*Institut rayonnement-matiere de Saclay (Iramis), CEA Saclay Bat 524, Gif-sur-Yvette cedex, F-91191, France*
[8]*Helmholtz-Zentrum Berlin für Materialien und Energie GmbH, Albert-Einstein-Straße 15, D-12489 Berlin, Germany*
[9]*Institut für Physik und CINSaT, Universität Kassel, Heinrich-Plett-Str. 40, 34132 Kassel, Germany*
[10]*Department of Physics, Lund University, PO Box 118, SE-221 00 Lund, Sweden*
[11]*Department of Computer Science and Applied Physics, Galway-Mayo Institute of Technology, Galway Campus, T91 T8NW Galway, Ireland*
[12]*Department of Physics and Astronomy, Drake University, Des Moines, Iowa 50311, USA*

(Received 4 December 2020; revised 7 February 2021; accepted 10 February 2021; published 26 February 2021)

We report angle-resolved measurements on photoelectrons emitted upon near-threshold two-photon double ionization (TPDI) of Kr irradiated by free-electron laser (FEL) pulses. These photoelectron angular distributions (PADs) are compared with the results of semirelativistic *R*-matrix calculations. As reported by Augustin *et al.* [Phys. Rev. A **98**, 033408 (2018)], it is found that the presence of autoionizing resonances within the bandwidth of the exciting FEL pulse strongly influences the PADs. In contrast to measurements on lower-*Z* targets such as Ne and Ar, the larger spin-orbit interaction, inherent in 4*p*-subshell hole states of Kr, permits us to resolve and study PADs associated with some of the fine-structure components of the Kr^+ and Kr^{2+} ions.

DOI: 10.1103/PhysRevA.103.022832

I. INTRODUCTION

Atomic valence shell photoionization in intense laser fields has been extensively investigated over the past four decades by means of table-top lasers operating in the near-infrared and visible spectral regions. Nonlinear processes such as above-threshold ionization (ATI) [1] and multiphoton ionization [2] were observed for the first time in pioneering studies. The absence of sufficiently intense, short-wavelength radiation prevented the observation of nonlinear processes involving inner-shell electrons during this early period. Gradually, the situation improved as progress on laser-driven high harmonic generation (HHG) sources [3], allowed for the investigation of nonlinear processes such as two-photon single and double ionization [4–8], including, most recently, angle-resolved photoelectron studies [9].

The advent of free-electron lasers (FELs) represented a landmark in delivering vacuum ultraviolet (VUV) and extreme ultraviolet (XUV) pulses of high enough brightness [10,11] to induce and probe nonlinear processes involving inner-shell electrons (see, e.g., Refs. [12,13]). Ion [14] and electron [15] time-of-flight (TOF) spectroscopy was used in order to illustrate several light-induced atomic processes such as two-photon excitation via inner-shell resonances [16–18], shake-up and shake-off effects in atomic ions [19] and the presence of sidebands in the photoelectron spectra of two-color photoionization experiments [20–23].

The interplay between the sequential and direct nature of atomic photoionization has been demonstrated in several experiments performed over the past decade [24,25]. However, most experiments were carried out using ion TOF detection and very few angle-resolved measurements have been made to date. Braune and his coworkers [26,27] were the first team to perform angle-resolved photoelectron spectroscopy measurements on electrons produced by sequential two-photon double ionization in Ne, Ar, and Kr. In that case the photon energy of the FLASH FEL was tuned to five specific values in the range from 38 to 91 eV and the experimental results were compared with theoretical calculations provided by Fritzsche *et al.* [28,29] and Kheifets *et al.* [30]. A few other experiments on PADs in multiphoton double ionization in FEL fields exist [31–36]. The early studies on the sequential ionization in noble gases are outlined in Ref. [37]. A "complete" experiment, based on PAD measurements, was performed on the sequential two-photon double ionization of neon in the region of one-particle one-hole autoionizing states (AISs) of Ne^+ [38]. Furthermore, the effect of autoionizing Rydberg resonances on the angular distribution of photoelectrons in

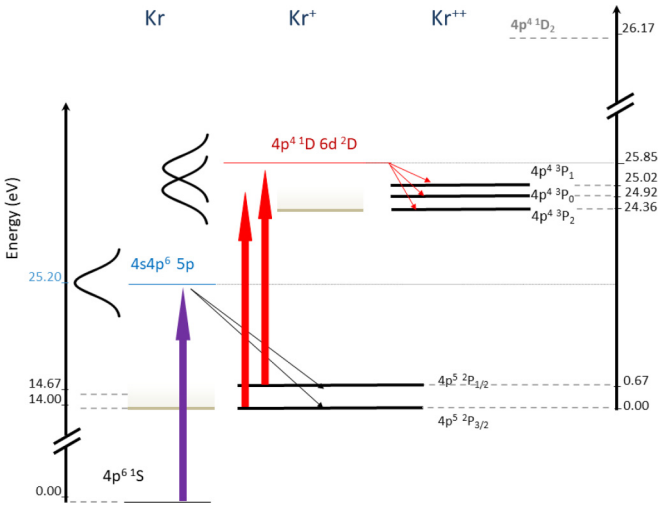

FIG. 1. Partial energy-level diagram corresponding to the conditions chosen in our experiment. The vertical arrows represent the absorbed FEL photons for the first and the second-ionization step. The slanted arrows represent the relaxation upon absorption of a FEL photon. Convolution with a Gaussian function is required in order to account for the inherent bandwidth of the FEL photon energy. The energy bandwidth is represented by the black curves.

TPDI was treated theoretically in Ref. [39]. The present work was motivated by an experiment on TPDI in Ar [31] where only the ^3P term of the $rm3p^4$ configuration of Ar^{2+} was accessible to the FEL photon energy used. The ^2P term of the $3p^5$ configuration was also accessible in the first step but it was not possible to resolve the individual $^3P_{2,1,0}$ spin-orbit split terms.

Here, we report angle-resolved measurements on photoelectrons ejected upon sequential two-photon double ionization of Kr. In this study the FEL photon energy was set at 25.2 eV, slightly above the $4p$ ionization threshold for Kr^+ (at 24.36 eV). Upon absorption of a 25.2 eV FEL photon one $4p$ electron is emitted, populating either of the two $4p^5\ ^2P_{3/2,1/2}$ spin-orbit split states. In the second-ionization step, one more electron is emitted and the Kr^{2+} ion ends up in any of the $4p^4\ ^3P_{2,1,0}$ terms. This is the only energetically available pathway, since there is not enough energy available to reach the $4p^4\ ^1D_2$ state, as can be seen in the partial energy diagram in Fig. 1. The $^1S_0$ state is not shown in the figure but lies at even higher energy (ca. 28.46 eV). Setting the photon energy close to the Kr^+ ionization threshold means that only the ^3P term of the resulting Kr^{2+} $(4p^4)$ configuration is accessible, as in experiment [31]. However, in contrast to Ref. [31], for single ionization of Kr we can resolve the individual spin-orbit split components of the $4p^5\ ^2P$ term so that we can compare measured anisotropy parameters with computed ones for each total angular momentum J. Also, we are able to resolve some of the fine structure associated with the second-ionization step, $4p^5\ ^2P_J$-$4p^4\ ^3P_{J'}$. As in Ref. [31], we find that accounting for the presence of the Rydberg structure within the excitation bandwidth of the FEL brings theoretical and experimental PADs into better agreement except for one second step ionization pathway, namely $4p^5\ ^2P_{3/2}$ -$4p^4\ ^3P_{1,0}$. We believe that extending these studies to Kr, thereby allowing us to resolve the electron PADs corresponding to some of the fine structure on both the first and second-ionization steps, represents another important step towards a more complete understanding of TPDI and the role of autoionizing states on this fundamental process.

In Sec. II the underlying theory is outlined, in Sec. III the experiment is briefly described, in Sec. IV the results are presented and discussed, while in Sec. V some conclusions are drawn.

II. THEORY

A detailed description of the theoretical work performed by Grum-Grzhimailo and his coworkers in order to model the angular distributions in the sequential two-photon double ionization is given in Ref. [37]. In brief, the photoelectron differential cross section in the dipole approximation can be expressed in terms of Legendre polynomials:

$$\frac{d\sigma}{d\Omega} = \frac{\sigma}{4\pi} \sum_{k=0}^{\infty} a_k P_k(\cos\theta), \tag{1}$$

where k takes even values, σ denotes the photoionization cross section, and θ corresponds to the angle determined by the direction of the emitted photoelectron and the polarization vector of the incident radiation.

For ionization of an isotropic target by absorption of one photon, it holds that $a_k = 0$ for $k > 2$ and the photoelectron differential cross section is given by [40]

$$\frac{d\sigma(E)}{d\omega} = \frac{\sigma(E)}{4\pi}[1 + \beta_2(E)P_2(\cos\theta)], \tag{2}$$

where $\beta_2(E)$ is the anisotropy parameter for such single-photon ionization.

As stated in the introduction, the two-photon double-ionization process takes place in two steps. In the first step a FEL photon ionizes the neutral atom to form a singly charged ion. In a further step, a second electron is released by absorption of another FEL photon from the same pulse, leading to a doubly charged ion. In that case, the extra term β_4 introduces the fourth order Legendre polynomial which is required in order to account for the polarization of the intermediate ionic state [41].

For sequential TPDI the photoelectron differential cross section becomes

$$\frac{d\sigma(E)}{d\omega} = \frac{\sigma(E)}{4\pi}[1 + \beta_2(E)P_2(\cos\theta) + \beta_4(E)P_4(\cos\theta)]. \tag{3}$$

Note that the *double* ionization Eq. (3) holds for electrons from *both* ionization steps with their own anisotropy parameters β_2 and β_4, as discussed in Refs. [29,31,35]. The cross sections and the anisotropy parameters are expressed in terms of partial photoionization amplitudes, as derived in Ref. [29].

To calculate the amplitudes we used an approach based on a semirelativistic version of the *B*-spline *R*-matrix code [42,43], taking full account of the nonorthogonality of the electron orbitals and diagonalization of the Breit-Pauli Hamiltonian. For the atomic Kr ionization, the initial state was obtained by a full self-consistent calculation of

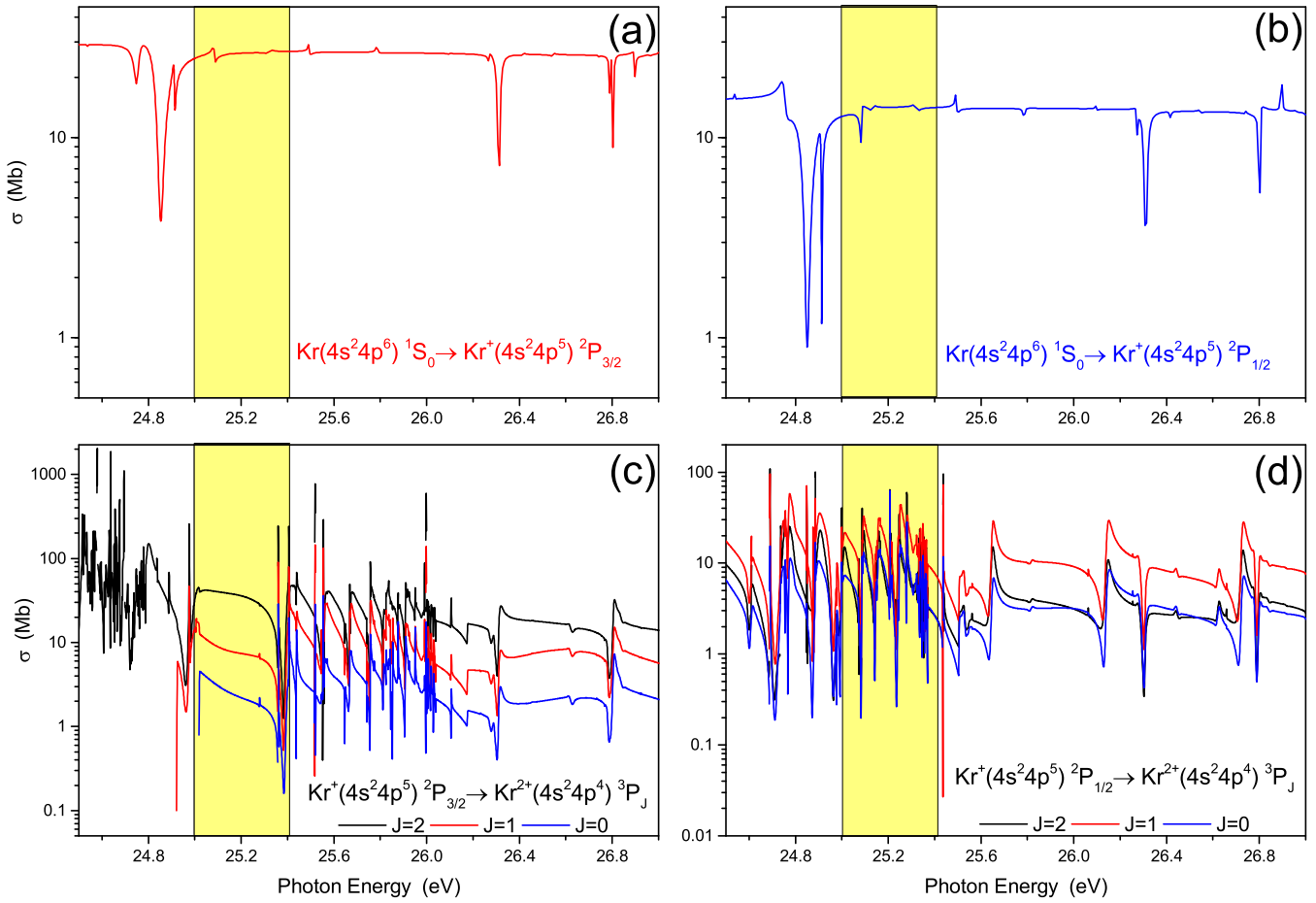

FIG. 2. (a), (b) Calculated photoionization cross sections for neutral Kr showing the region of the $4s^{-1}np$ resonance series. The $4s^{-1}np$ states strongly influence the $Kr^{+}4s^{2}4p^{5}\,{}^{2}P_{3/2}$ or $Kr^{+}4s^{2}4p^{5}\,{}^{2}P_{1/2}$ cross section, respectively. (c), (d) Calculated photoionization cross sections for singly ionized Kr showing the region of the $(4p^{4}\,{}^{1}D)ns, nd$ resonance series. The upper members of the series $(4p^{4}\,{}^{1}D)ns$ ($n \geqslant 9$) and $(4p^{4}\,{}^{1}D)nd$ ($n \geqslant 6$) decay to the $Kr^{2+}4s^{-1}4p^{4}\,{}^{3}P_{2,1,0}$ states. The shaded region corresponds to the FEL bandwidth.

the [Ar] $3d^{10}4s^{2}4p^{6}$ configuration, with subsequent freezing of all orbitals, except $4s$ and $4p$, and mixing ^{1}S terms of the $4s^{2}4p^{6} + 4s^{2}4p^{5}5p + 4s4p^{6}5s + 4s4p^{5}4d5p + 4p^{6}4d^{2} + 4s^{2}4p^{4}4d5s$ configurations, in order to optimize the $5s$, $5p$, and $4d$ correlation orbitals on the energy of the ground state. The final ionic states were represented by mixed thresholds with configurations $4s^{2}4p^{5}$, $4s4p^{6}$, $4s4p^{4}5s$, $4s4p^{4}4d$, $4s4p^{4}5p$, including all terms with $J = 1/2,\ 3/2,\ 5/2$. Here the $4s$ and $4p$ orbitals were varied independently for each LS term, while the inner orbitals up to $3d$ were obtained in the $[\mathrm{Ar}]3d^{10}4s^{2}4p^{5}$ calculation and were frozen. Note that, for the angular distribution of the second electron, only the alignment of the $4s^{2}4p^{5}\,{}^{2}P_{3/2}$ intermediate is needed in the narrow region between 25.0 and 25.4 eV photon energy, because the influence of the $3d$ subshell begins at higher energies [44]. For the second step where only the lowest $Kr^{2+}4p^{4}\,{}^{3}P_{J}$ ($J = 0, 1, 2$) thresholds are opened, the present theory accounted for the $4s^{2}4p^{4}\,{}^{1}S_{0}\,{}^{3}P_{0,1,2}$, $^{1}D_{2}$ and $4s4p^{5}\,{}^{1}P_{1}$, $^{3}P_{0,1,2}$ mixed thresholds. The initial state was a pure $Kr^{+}4p^{5}\,{}^{2}P_{1/2,3/2}$ doublet state. All the orbitals were obtained independently for each LS term of the above configurations. Experimental energies of the thresholds were used.

III. EXPERIMENT

The experiment employed the CAMP instrument installed at the beamline BL1 [45] at FLASH FEL at DESY [10]. CAMP houses a double-sided (electron and ion imaging) VMI spectrometer where the photoelectron spectra are registered by means of a multichannel plate/phosphor (MCP/phosphor) screen and a CCD camera operating at a frame readout rate of 10 frames per second (fps). This arrangement offers detection of electrons in a full 4π solid angle, and the spectrometer provides a mean electron energy resolution of approximately 0.3 eV over the electron kinetic-energy range of interest here (namely, 0–12 eV). To reconstruct the slices of the three-dimensional (3D) photoelectron angular distributions out of the two-dimensional (2D) VMI images, three alternative methods of the inverse Abel transformation have been applied: the BASEX method [46], direct integration of the Abel integral [46], and an iterative approach [47], which all gave identical results.

The main experimental parameters are reported in a previous work [20]. In brief, the FEL photon energy was set at 25.2 eV, exhibiting an inherent bandwidth of 0.3–0.4 eV (full width at half maximum, FWHM). Importantly, the FLASH

FEL was operated in self-amplified spontaneous emission (SASE) mode, thus exhibiting a spiky intensity distribution of the extreme ultraviolet (XUV) pulse (see, e.g., Ref. [20]). Hence the pulse duration was estimated to vary from 60 to 140 fs with a mean value of 100 fs (FWHM), and the pulse energy at the focus ranged from ≈ 2 μJ to ≈ 6 μJ. The focal spot diameter was estimated to be approximately 20 μm, at which diameter, the peak intensity present in our experiments is $\approx 2.0 \times 10^{13}$ W/cm^2 for a pulse energy of 6 μJ and a duration of 100 fs.

IV. RESULTS AND DISCUSSION

In Figs. 2(a) and 2(b) the calculated (partial) photoionization cross sections for atomic Kr including the $4s^{-1}np$ states which decay to the two first ionization thresholds of Kr, namely, the $^2P_{3/2}$ [Fig. 2(a)] and the $^2P_{1/2}$ [Fig. 2(b)] limits, are shown along with the total cross section. The calculations show some weaker structures in the vicinity of the $4s \rightarrow 5p$ resonances. These have been observed in high-resolution measurements [48,49] and are due to doubly excited states that gain oscillator strength via configuration interaction with the singly excited $4s^{-1}np$ states.

Figures 2(c) and 2(d) show the calculated photoionization cross sections for Kr^+ including the $4p^5\,^2P_{3/2,1/2} \longrightarrow 4p^4\,^3P_{2,1,0}\,ns, nd$ series. These more elaborate evaluations included the following mixed Kr^{2+} thresholds: $4P^4\,^3P_{0,1,2}, ^1D_2, ^1S_0$; $4s^{-1}4p^5\,^3P_{0,1,2}, ^1P_1$; $4s^{-2}4p^6\,^1S_0$. The results are in good agreement with experiment [50] and calculations [51] for the total photoionization cross section.

At the chosen photon energy, ionization from the $^2P_{3/2}$ component is affected by a few lowest AIS from the $4p^4\,^1D\,nd$ series ($n = 6, 7$), and ionization from the $^2P_{1/2}$ component is affected by the highest AIS of this series. The series $4p^4\,^1S\,nd, ns$ seen at the photon energies above 26.0 eV in Fig. 2(c) and 25.4 eV in Fig. 2(d) do not contribute to the measured PADs. It is clear that, in the first ionization step ($Kr \rightarrow Kr^+$) and especially in the second step ($Kr^+ \rightarrow Kr^{2+}$), the density of rapidly varying resonance structure will lead to rapid fluctuations in other key atomic parameters, especially here the anisotropy parameters characterizing the angular distributions of the emitted photoelectrons.

In Fig. 3(a) an angle-integrated photoelectron spectrum is shown for a FEL intensity $\approx 2 \times 10^{13}$ W/cm^2, along with a simulated spectrum [Fig. 3(b)] for a photon energy of 25.2 eV, convolved with a Gaussian profile to account for the instrumental broadening of the experimental data. The first point to be made is that the $^2P_{3/2}$ and $^2P_{1/2}$ components in the first ionization step are distinguishable at $\approx$11.20 eV and $\approx$10.50 eV, respectively. In addition, three more photoelectron peaks associated with the second-ionization step are discernible. More specifically, the peak at $\approx$1.45 eV corresponds to the $Kr^+4s^24p^5\,^2P_{1/2} \longrightarrow Kr^{2+}4s^24p^4\,^3P_2$ transition, the peak at $\approx$0.25 eV to the $Kr^+4s^24p^5\,^2P_{3/2} \longrightarrow Kr^{2+}4s^24p^4\,^3P_{1,0}$ transition, whereas the photoelectron peak at $\approx$0.85 eV incorporates contributions from both the $Kr^+4s^24p^5\,^2P_{1/2} \longrightarrow Kr^{2+}4s^24p^4\,^3P_{1,0}$ and $Kr^+4s^24p^5\,^2P_{3/2} \longrightarrow Kr^{2+}4s^24p^4\,^3P_2$ transitions. The theoretically simulated spectrum is in good agreement with the experimentally acquired data, with respect to both the positions and the relative intensities of the photoelectron peaks. The spiky structure of the main photoelectron lines is generated by underlying Rydberg series of autoionizing states; however, such structure gets washed out by the instrumental broadening in the experiment.

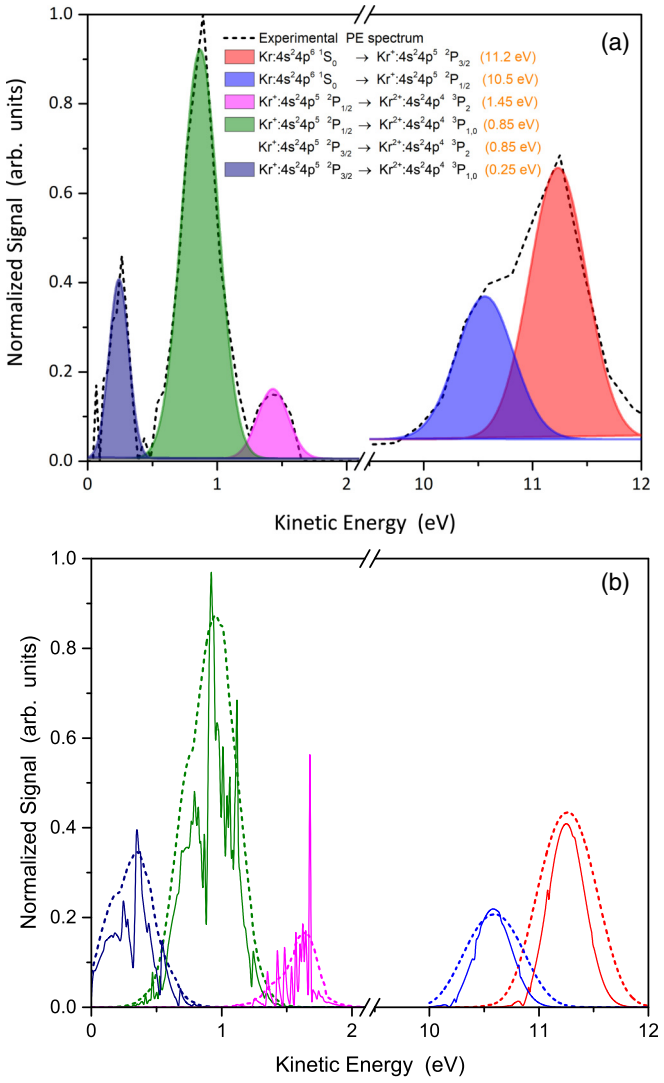

FIG. 3. (a) Experimental angle-averaged photoelectron spectrum for a FEL intensity $\approx 2.5 \times 10^{13}$ W/cm^2. (b) Theoretically simulated photoelectron spectrum for a FEL photon energy of 25.2 eV. The dashed lines correspond to the convolution of the calculated spectrum with a Gaussian profile, of 0.3 eV (FWHM) and 0.6 eV (FWHM) for the second- and first-ionization step, respectively.

Moving on to the angle-resolved measurements for the first step, Fig. 4 shows the computed β_2 anisotropy parameter as a function of the photoelectron energy in the region of interest here. The two curves, dashed red and solid blue, correspond to ionization to $4p^5\,^2P_{3/2}$ and $4p^5\,^2P_{1/2}$ ionic states, respectively, without convolution. As one would expect, the anisotropy parameters change quite rapidly in the resonance region. Importantly, the theoretical curve for the β_2 anisotropy parameter drops down to zero at resonance energies corresponding to ionization from both the $^2P_{3/2}$ (dashed red) and the $^2P_{1/2}$ line (solid blue) and increases for higher electron energies, up

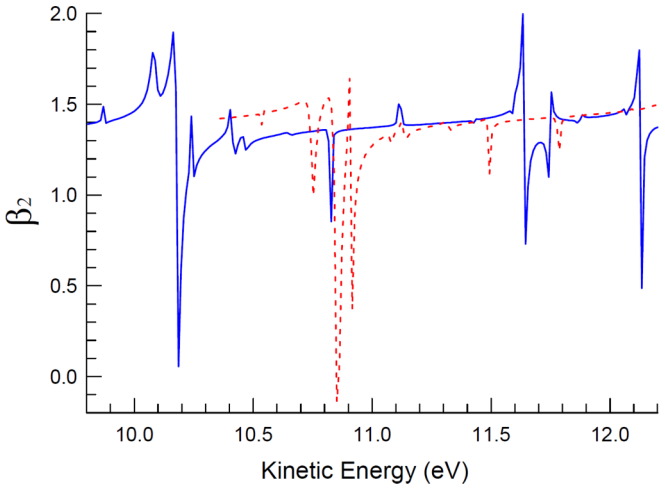

FIG. 4. Calculated anisotropy parameter of the first ionization step of the TPDI of Kr as a function of photoelectron energy for electrons corresponding ionization to $4p^5\,^2P_{3/2}$ state (red dashed line) and to $4p^5\,^2P_{1/2}$ (blue solid line).

to nonresonant values of $\beta_2 \approx 1.5$, well known from previous experimental studies [48,52]. Furthermore, theoretically calculated β_2 values of approximately 1.25, closer to the values obtained in this work, have been reported [53]. To compare the theoretical angular distributions with experiment, one has to multiply the calculated photon-energy and angle-dependent electron signal by the normalized envelope of the FEL pulse. The result is then convoluted with the electron detector resolution. The results of this procedure together with the experimental data are shown in Figs. 5 and 6.

We show in Fig. 5 the PADs for the Kr $^1S_0$ to $Kr^+\,^2P_{1/2}$ (top panel) and $^2P_{3/2}$ (bottom panel) ionization channels. The measured values correspond to the black data points. The dashed curve is the result of fitting Eq. (3) to the experimental data for each ionization pathway. The dotted curve in each case is the calculated PAD (see Ref. [28]) without accounting for resonantly excited states that lie within the bandwidth of the FEL [the shaded band or stripe shown in Figs. 2(a) and 2(b)]. The solid curve corresponds to the theoretically calculated PADs after accounting for Rydberg states in the excitation photon energy band of interest here. It is clear that Rydberg states play an important role in this case as they did in Ar [31], albeit the PAD was measured for the ^2P term but not its fine-structure components in the latter experiment. Inclusion of the resonances lying within the FEL excitation bandwidth results in a reduction in the computed β_2 values so that they are closer to the measured values of 1.20 ± 0.06 for the Kr $^1S_0 \rightarrow Kr^+\,^2P_{3/2}$ photoionization pathway and 1.20 ± 0.10 for the Kr $^1S_0 \rightarrow Kr^+\,^2P_{1/2}$ channel. The value of the anisotropy parameter for the theoretical curve lies above the experimental value because the theoretically computed resonance is located at a lower energy than the measured value. Hence one should use the theoretically computed value but shifted to lower electron energy (11.0 eV instead of 11.1 eV in Fig. 4) where β_2 decreases in the resonance. Furthermore, the optimum fitting of the experimental angular distributions resulted in small negative β_4 values. More specifically, we obtained values of $\beta_4 = -0.09 \pm 0.06$ and

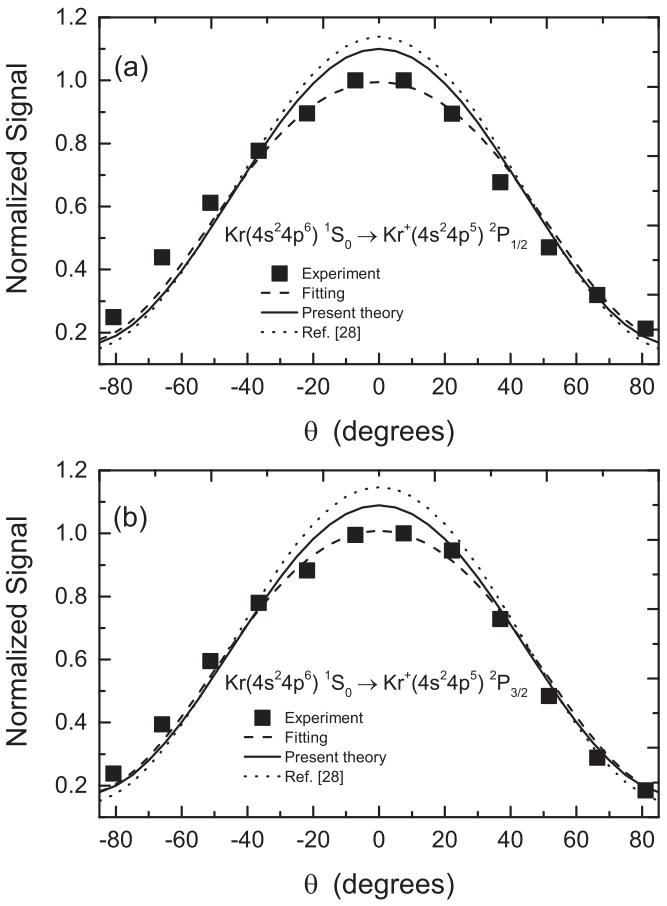

FIG. 5. Photoelectron angular distributions for the two open channels of the first ionization step and for a FEL intensity of $\approx 2.5 \times 10^{13}$ W/cm^2. The top panel corresponds to the Kr $^1S_0 \rightarrow Kr^+\,^2P_{1/2}$ channel and the bottom panel to the Kr $^1S_0 \rightarrow Kr^+\,^2P_{3/2}$ channel.

$\beta_4 = -0.11 \pm 0.10$ for the $^2P_{3/2}$ and the $^2P_{1/2}$ components, respectively. It is clear that the experimental β_4 values have quite large errors associated with them and so we cannot, at this stage, rule out the possibility that they may in fact be equal to zero. Note that any model based on the lowest nonvanishing order perturbation theory predicts negligible or zero β_4 values [54].

The computed anisotropy parameters for the second-step ionization are plotted in Fig. 7 as a function of the photoelectron energy, in the region of interest indicated in Figs. 2(c) and 2(d). There are dramatic fluctuations in the anisotropy parameters caused by the resonances shown in Fig. 2. However, the theoretical values presented in Table I take into account both the spectral width of the photon beam and the spectral resolution of the spectrometer, which leads to a smoothing. Even in this case the impact of the discrete structure on the asymmetry parameters, especially the β_2 values is very significant. The β_4 parameters are predicted to be small in the second-step ionization, due to small alignment of the intermediate $Kr^+\,^2P_{3/2}$ state [28].

Concerning the asterisk in Table I, the *R*-matrix calculations near the thresholds of the Rydberg series were not completely reliable. Note that there are no decay channels in the isolated ions for these resonances to be further broadened

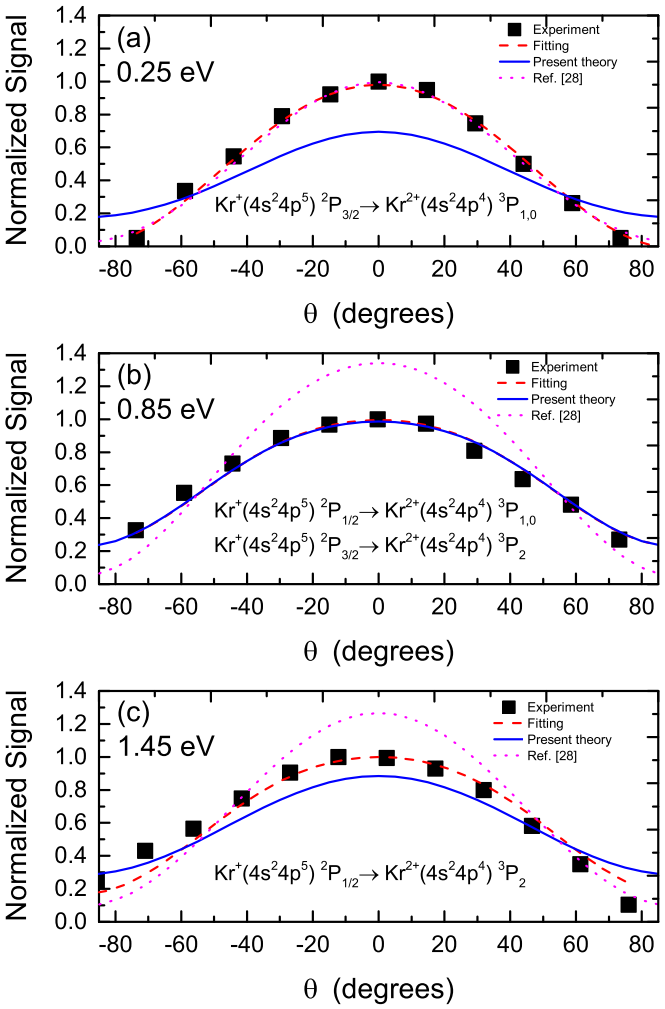

FIG. 6. Photoelectron angular distributions for the three open channels of the second-ionization step and for a FEL intensity of $\approx 2.5 \times 10^{13}$ W/cm^2. Panel (a) corresponds to the $Kr^+\ ^2P_{3/2} \rightarrow Kr^{2+}\ ^3P_{1,0}$ channel, panel (b) to the $Kr^+\ ^2P_{1/2} \rightarrow Kr^{2+}\ ^3P_{1,0}$ and $Kr^+\ ^2P_{3/2} \rightarrow Kr^{2+}\ ^3P_2$ channels, and panel (c) to the $Kr^+\ ^2P_{1/2} \rightarrow Kr^{2+}\ ^3P_2$ channel.

and thus smooth the resonance manifold. Assuming that the profile of the resonances is similar along the Rydberg series [55], we theoretically interpolated the series up to threshold and used this interpolation in the corresponding energy region. Additionally, the experimental data represent the average of thousands of FEL shots with spiky spectral distributions which vary randomly from shot to shot with respect to intensity and overall (envelope) spectral distribution. Thus the undetermined structure of the SASE pulse may also influence the convolution procedure in this critical region. The exclusion of resonance structure resulted in β_4 values of -0.1, 0.1, and zero for electron kinetic energies of 0.25, 0.85, and 1.45 eV, respectively. Thus it does not significantly affect the computed β_4 values.

Turning now to a comparison with the experiment, we show in Fig. 6 the measured PADs for the three photoelectron features observed to lie at kinetic energies of 0.25, 0.85, and 1.45 eV (Fig. 3). The measured PADs are shown as black data points and the dashed red curves are obtained by fitting

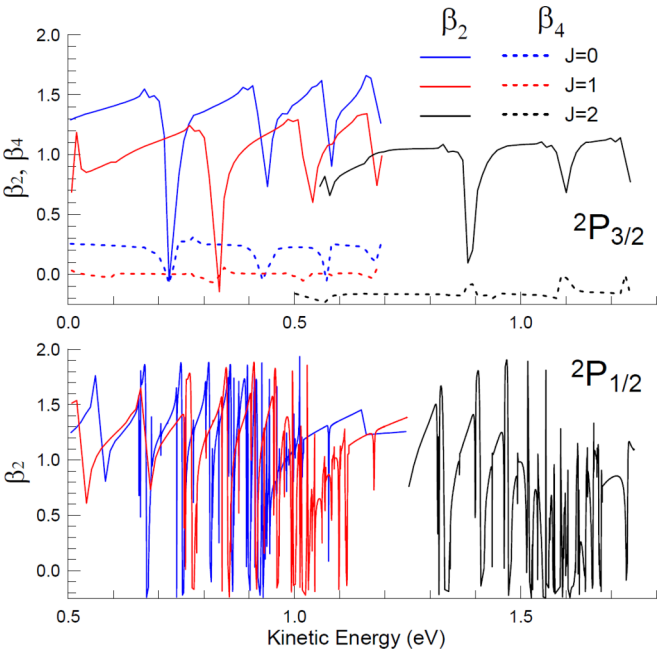

FIG. 7. Calculated anisotropy parameters β_2, β_4 for ionization from $Kr^+\ 4p^5\ ^2P_{3/2}$ (upper) and β_2 for ionization from $^2P_{1/2}$ (lower) for the three components of the second-ionization step, $Kr^{2+}4p^4\ ^3P_{0,1,2}$, and for a FEL photon energy set at 25.2 eV (see text).

Eq. (3) to them. The dotted pink and solid blue curves are the computed PADs in the absence and presence, respectively, of resonances. In the case of the features at 0.85 and 1.45 eV [Figs. 6(b) and 6(c), respectively], it can be stated that the inclusion of resonance structure improves the agreement with the experiment (as it did in the first-step ionization).

The only PAD with single initial and final states (at the fine structure level) is that for the photoelectron line at 1.45 eV [Fig. 6(c)]. As is clear from Fig. 2(c) there is a very densely packed discrete resonance structure that can be excited out of the $Kr^+4s^24p^5\ ^2P_{1/2}$ state by the FEL and so its inclusion can be expected to result in a real improvement of the agreement between theory and experiment. In Fig. 6(b), we observe an excellent agreement between experiment and theory for the blended features at 0.85 eV which yield two overlapping PADs. In that case, we were not able to separate the resonances sufficiently well (post-deconvolution of the instrumental broadening) and so could not obtain two separate PADs with good signal-to-noise statistics for reliable

TABLE I. The angular anisotropy parameters for different photoelectron energies calculated at a photon energy of 25.2 eV, with a FEL pulse of FWHM = 0.4 eV and the FWHM of the electron detector resolution set at 0.6 and 0.3 eV for the first- and second-step electrons, respectively. The asterisk sign is explained in the text.

	First step		Second step		
E_e, eV	11.2	10.5	1.4*	0.8	0.2
β_2	1.29	1.32	0.93	1.0	1.03
β_4			−0.02	−0.13	0.08

extraction of asymmetry parameters. However, it appears that inclusion of resonances has a very large part to play in that improvement between experiment and theory.

The most puzzling result concerns the peak at 0.25 eV [Fig. 6(a)] for which there is one Kr^+ fine-structure component in the initial state ($^2P_{3/2}$) but two (unresolved) fine-structure components $^3P_{1,0}$ in the final Kr^{2+} state. In this case the best agreement is obtained by computing the asymmetry parameters and corresponding PAD without accounting for resonances. We believe that the reason of this unexpected result at the lowest electron energy is a very high sensitivity of the phases of the ionization amplitudes at the threshold to the model, reinforced by the resonances. The current theory may need further improvement, including some additional electron correlation and accounting for the unknown spiky structure of the pulses, as mentioned above, while the model without AIS may give here an accidental agreement with the experiment. For the record the experimentally extracted asymmetry parameters are $\beta_2 = 2.00 \pm 0.10$ and $\beta_4 = -0.08 \pm 0.07$ for the 0.25 eV line, $\beta_2 = 1.03 \pm 0.07$ and $\beta_4 = -0.12 \pm 0.06$ for the 0.85 eV line, $\beta_2 = 1.19 \pm 0.12$, $\beta_4 = -0.15 \pm 0.12$ for the 1.45 eV line. It should be noted that the errors are statistical and obtained from the fits to the PADs.

V. CONCLUSIONS

To summarize, we report angle-integrated and angle-resolved photoelectron measurements for sequential two-photon double ionization of Kr for a FEL photon energy near the second-ionization threshold. The choice of Kr permitted us to resolve fine structure in the initial and final states in the first-step ionization pathways and to do so partially in the second step. Measurements were accompanied by theoretical calculations. The angle-integrated photoelectron spectra exhibit good agreement with theory, which was able to reproduce the energies and relative intensities of the photoelectron peaks. Angle-resolved spectra were used to extract the anisotropy parameters which were then compared with the theoretical values. Our findings once again highlight the importance of resonances, particularly on angle-resolved measurements where resonance related signatures are prominent. Clear improvements for the future would involve measurements at a narrow bandwidth seeded FEL to tune on or off resonance and explore the effects of resonances on PADs in ions as well as the use of coincidence measurements on both first- and second-step electrons so that correlations between them could be measured.

ACKNOWLEDGMENTS

We want to acknowledge the work of the scientific and technical team at FLASH. We acknowledge the Max Planck Society for funding the development and the initial operation of the CAMP endstation within the Max Planck Advanced Study Group at CFEL and for providing this equipment for CAMP@FLASH. The installation of CAMP@FLASH was partially funded by the BMBF grants 05K10KT2, 05K13KT2, 05K16KT3, and 05K10KTB from FSP-302. E.V.G. and M.D.K. acknowledge funding from the Basis Foundation under the program "Junior Leader." A.N.G.-G, S.M.B., E.V.G., and M.D.K. acknowledge funding by Russian Federation for Basic Research (RFBR) under the research project No. 20-52-12023. M.I. acknowledges funding from the Volkswagen foundation within a Peter Paul Ewald-Fellowship. P.J. acknowledges support from the Swedish Research Council and the Swedish Foundation for Strategic Research. M.M. and T.M. acknowledge support from the Deutsche Forschungsgemeinschaft (DFG) under Grant no. SFB925/1. The DCU group was supported by the Education, Audio-visual and Culture Executive Agency (EACEA) Erasmus Mundus Joint Doctorate Programme EXTATIC, Project No. 2013 0033 and Science Foundation Ireland Grants No. 16/RI/3696 and No. 19/FFP/6956. Work associated with EU H2020 COST Action No. CA17126 (TUMIEE) and SEAI Grant No. 19/RDD/556.

[1] P. Agostini, F. Fabre, G. Mainfray, G. Petite, and N. K. Rahman, Phys. Rev. Lett. **42**, 1127 (1979).

[2] G. Mainfray and G. Manus, Rep. Prog. Phys. **54**, 1333 (1991).

[3] T. Pfeifer, C. Spielmann, and G. Gerber, Rep. Prog. Phys. **69**, 443 (2006).

[4] E. P. Benis, D. Charalambidis, T. N. Kitsopoulos, G. D. Tsakiris, and P. Tzallas, Phys. Rev. A **74**, 051402(R) (2006).

[5] N. A. Papadogiannis, L. A. A. Nikolopoulos, D. Charalambidis, G. D. Tsakiris, P. Tzallas, and K. Witte, Phys. Rev. Lett. **90**, 133902 (2003).

[6] T. Sekikawa, A. Kosuge, T. Kanai, and S. Watanabe, Nature (London) **432**, 605 (2004).

[7] Y. Nabekawa, H. Hasegawa, E. J. Takahashi, and K. Midorikawa, Phys. Rev. Lett. **94**, 043001 (2005).

[8] B. Manschwetus, L. Rading, F. Campi, S. Maclot, H. Coudert-Alteirac, J. Lahl, H. Wikmark, P. Rudawski, C. M. Heyl, B. Farkas, T. Mohamed, A. L'Huillier, and P. Johnsson, Phys. Rev. A **93**, 061402(R) (2016).

[9] K. A. Larsen, D. S. Slaughter, and T. Weber, Phys. Rev. A **101**, 061402(R) (2020).

[10] W. Ackermann, G. Asova, V. Ayvazyan, A. Azima, N. Baboi, J. Bähr, V. Balandin, B. Beutner, A. Brandt, A. Bolzmann, R. Brinkmann, O. I. Brovko, M. Castellano, P. Castro, L. Catani, E. Chiadroni, S. Choroba, A. Cianchi, J. T. Costello, D. Cubaynes *et al.*, Nat. Photon. **1**, 336 (2007).

[11] E. Allaria, R. Appio, L. Badano, W. Barletta, S. Bassanese, S. Biedron, A. Borga, E. Busetto, D. Castronovo, P. Cinquegrana, S. Cleva, D. Cocco, M. Cornacchia, P. Craievich, I. Cudin, G. D'Auria, M. Dal Forno, M. Danailov, R. De Monte, G. De Ninno, P. Delgiusto, A. Demidovich *et al.*, Nat. Photon. **6**, 699 (2012).

[12] N. Berrah, J. Bozek, J. Costello, S. Düsterer, L. Fang, J. Feldhaus, H. Fukuzawa, M. Hoener, Y. Jiang, P. Johnsson, E. Kennedy, M. Meyer, R. Moshammer, P. Radcliffe, M. Richter, A. Rouzée, A. Rudenko, A. Sorokin, K. Tiedtke, K. Ueda, J. Ullrich, and M. Vrakking, J. Mod. Opt. **57**, 1015 (2010).

[13] J. Marangos, Contemp. Phys. **52**, 551 (2011).

[14] A. A. Sorokin, S. V. Bobashev, T. Feigl, K. Tiedtke, H. Wabnitz, and M. Richter, Phys. Rev. Lett. **99**, 213002 (2007).

[15] T. Laarmann, A. R. B. de Castro, P. Gürtler, W. Laasch, J. Schulz, H. Wabnitz, and T. Möller, Phys. Rev. A **72**, 023409 (2005).

[16] M. Meyer, D. Cubaynes, V. Richardson, J. T. Costello, P. Radcliffe, W. B. Li, S. Düsterer, S. Fritzsche, A. Mihelic, K. G. Papamihail, and P. Lambropoulos, Phys. Rev. Lett. **104**, 213001 (2010).

[17] M. Richter, M. Y. Amusia, S. V. Bobashev, T. Feigl, P. N. Juranić, M. Martins, A. A. Sorokin, and K. Tiedtke, Phys. Rev. Lett. **102**, 163002 (2009).

[18] V. Richardson, J. T. Costello, D. Cubaynes, S. Düsterer, J. Feldhaus, H. W. van der Hart, P. Juranić, W. B. Li, M. Meyer, M. Richter, A. A. Sorokin, and K. Tiedke, Phys. Rev. Lett. **105**, 013001 (2010).

[19] M. Ilchen, T. Mazza, E. T. Karamatskos, D. Markellos, S. Bakhtiarzadeh, A. J. Rafipoor, T. J. Kelly, N. Walsh, J. T. Costello, P. O'Keeffe, N. Gerken, M. Martins, P. Lambropoulos, and M. Meyer, Phys. Rev. A **94**, 013413 (2016).

[20] S. Düsterer, G. Hartmann, C. Bomme, R. Boll, J. T. Costello, B. Erk, A. De Fanis, M. Ilchen, P. Johnsson, T. J. Kelly, B. Manschwetus, T. Mazza, M. Meyer, C. Passow, D. Rompotis, L. Varvarezos, A. K. Kazansky, and N. M. Kabachnik, New J. Phys. **21**, 063034 (2019).

[21] P. Radcliffe, M. Arbeiter, W. B. Li, S. Düsterer, H. Redlin, P. Hayden, P. Hough, V. Richardson, J. T. Costello, T. Fennel, and M. Meyer, New J. Phys. **14**, 043008 (2012).

[22] M. Meyer, P. Radcliffe, T. Tschentscher, J. T. Costello, A. L. Cavalieri, I. Grguras, A. R. Maier, R. Kienberger, J. Bozek, C. Bostedt, S. Schorb, R. Coffee, M. Messerschmidt, C. Roedig, E. Sistrunk, L. F. Di Mauro, G. Doumy, K. Ueda, S. Wada, S. Düsterer, A. K. Kazansky, and N. M. Kabachnik, Phys. Rev. Lett. **108**, 063007 (2012).

[23] T. Mazza, M. Ilchen, A. Rafipoor, C. Callegari, P. Finetti, O. Plekan, K. Prince, R. Richter, A. Demidovich, C. Grazioli, L. Avaldi, P. Bolognesi, M. Coreno, P. O'Keeffe, M. Di Fraia, M. Devetta, Y. Ovcharenko, V. Lyamayev, S. Düsterer, K. Ueda, J. Costello, E. Gryzlova, S. Strakhova, A. Grum-Grzhimailo, A. Bozhevolnov, A. Kazansky, N. Kabachnik, and M. Meyer, J. Mod. Opt. **63**, 367 (2016).

[24] A. A. Sorokin, M. Wellhöfer, S. V. Bobashev, K. Tiedtke, and M. Richter, Phys. Rev. A **75**, 051402(R) (2007).

[25] R. Moshammer, Y. H. Jiang, L. Foucar, A. Rudenko, T. Ergler, C. D. Schröter, S. Lüdemann, K. Zrost, D. Fischer, J. Titze, T. Jahnke, M. Schöffler, T. Weber, R. Dörner, T. J. M. Zouros, A. Dorn, T. Ferger, K. U. Kühnel, S. Düsterer, R. Treusch, P. Radcliffe, E. Plönjes, and J. Ullrich, Phys. Rev. Lett. **98**, 203001 (2007).

[26] M. Braune, A. Reinköster, J. Viefhaus, B. Lohmann, and U. Becker, in *Proc. Int. Conf. on Photonic, Electronic and Atomic Collisions (ICPEAC)*, Freiburg, Fr034 (2007).

[27] M. Braune, G. Hartmann, M. Ilchen, A. Knie, T. Lischke, A. Reinköster, A. Meißner, S. Deinert, L. Glaser, O. Al-Dossary, A. Ehresmann, A. Kheifets, and J. Viefhaus, J. Mod. Opt. **63**, 324 (2016).

[28] S. Fritzsche, A. N. Grum-Grzhimailo, E. V. Gryzlova, and N. M. Kabachnik, J. Phys. B: At. Mol. Opt. Phys. **42**, 145602 (2009).

[29] S. Fritzsche, A. N. Grum-Grzhimailo, E. V. Gryzlova, and N. M. Kabachnik, J. Phys. B: At. Mol. Opt. Phys. **41**, 165601 (2008).

[30] A. S. Kheifets, J. Phys. B: At. Mol. Opt. Phys. **40**, F313 (2007).

[31] S. Augustin, M. Schulz, G. Schmid, K. Schnorr, E. V. Gryzlova, H. Lindenblatt, S. Meister, Y. F. Liu, F. Trost, L. Fechner, A. N. Grum-Grzhimailo, S. M. Burkov, M. Braune, R. Treusch, M. Gisselbrecht, C. D. Schröter, T. Pfeifer, and R. Moshammer, Phys. Rev. A **98**, 033408 (2018).

[32] A. Rouzée, P. Johnsson, E. V. Gryzlova, H. Fukuzawa, A. Yamada, W. Siu, Y. Huismans, E. Louis, F. Bijkerk, D. M. P. Holland, A. N. Grum-Grzhimailo, N. M. Kabachnik, M. J. J. Vrakking, and K. Ueda, Phys. Rev. A **83**, 031401(R) (2011).

[33] G. Hartmann, Ph.D. thesis, Technische Universitaet, Berlin, 2014.

[34] S. Mondal, R. Ma, K. Motomura, H. Fukuzawa, A. Yamada, K. Nagaya, S. Yase, Y. Mizoguchi, M. Yao, A. Rouzée, A. Hundertmark, M. J. J. Vrakking, P. Johnsson, M. Nagasono, K. Tono, T. Togashi, Y. Senba, H. Ohashi, M. Yabashi, T. Ishikawa, I. P. Sazhina, S. Fritzsche, N. M. Kabachnik, and K. Ueda, J. Phys. B: At. Mol. Opt. Phys. **46**, 164022 (2013).

[35] M. Kurka, A. Rudenko, L. Foucar, K. U. Kühnel, Y. H. Jiang, T. Ergler, T. Havermeier, M. Smolarski, S. Schössler, K. Cole, M. Schöffler, R. Dörner, M. Gensch, S. Düsterer, R. Treusch, S. Fritzsche, A. N. Grum-Grzhimailo, E. V. Gryzlova, N. M. Kabachnik, C. D. Schröter, R. Moshammer, and J. Ullrich, J. Phys. B: At. Mol. Opt. Phys. **42**, 141002 (2009).

[36] M. Kiselev, P. Carpeggiani, E. Gryzlova, S. Burkov, M. Reduzzi, A. Dubrouil, D. Faccial, M. Negro, K. Ueda, F. Frassetto, F. Stienkemeier, Y. Ovcharenko, M. Meyer, M. D. Fraia, O. Plekan, K. C. Prince, C. Callegari, G. Sansone, and A. N. Grum-Grzhimailo, J. Phys. B: At. Mol. Opt. Phys. **53**, 244006 (2020).

[37] A. N. Grum-Grzhimailo, E. V. Gryzlova, S. Fritzsche, and N. M. Kabachnik, J. Mod. Opt. **63**, 334 (2016).

[38] P. A. Carpeggiani, E. V. Gryzlova, M. Reduzzi, A. Dubrouil, D. Faccialá, M. Negro, K. Ueda, S. M. Burkov, F. Frassetto, F. Stienkemeier, Y. Ovcharenko, M. Meyer, O. Plekan, P. Finetti, K. C. Prince, C. Callegari, A. N. Grum-Grzhimailo, and G. Sansone, Nat. Phys. **15**, 170 (2019).

[39] E. V. Gryzlova, A. N. Grum-Grzhimailo, M. D. Kiselev, and S. M. Burkov, Eur. Phys. J. D **73**, 93 (2019).

[40] C. N. Yang, Phys. Rev. **74**, 764 (1948).

[41] V. V. Balashov, A. N. Grum-Grzhimailo, and N. M. Kabachnik, *Polarization and Correlation Phenomena in Atomic Collisions* (Springer US, Boston, 2000).

[42] O. Zatsarinny, Comput. Phys. Commun. **174**, 273 (2006).

[43] O. Zatsarinny and K. Bartschat, J. Phys. B: At. Mol. Opt. Phys. **46**, 112001 (2013).

[44] M. Y. Amusia, L. V. Chernysheva, and S. A. Sheinerman, Phys. Lett. A **82**, 171 (1981).

[45] B. Erk, J. P. Müller, C. Bomme, R. Boll, G. Brenner, H. N. Chapman, J. Correa, S. Düsterer, S. Dziarzhytski, S. Eisebitt, H. Graafsma, S. Grunewald, L. Gumprecht, R. Hartmann, G. Hauser, B. Keitel, C. von Korff Schmising, M. Kuhlmann, B. Manschwetus, L. Mercadier *et al.*, J. Synchrotron Radiat. **25**, 1529 (2018).

[46] V. Dribinski, A. Ossadtchi, V. A. Mandelshtam, and H. Reisler, Rev. Sci. Instrum. **73**, 2634 (2002).

[47] M. J. J. Vrakking, Rev. Sci. Instrum. **72**, 4084 (2001).

[48] M. G. Flemming, J.-Z. Wu, C. D. Caldwell, and M. O. Krause, Phys. Rev. A **44**, 1733 (1991).

[49] A. Neogi, E. T. Kennedy, J.-P. Mosnier, P. van Kampen, J. T. Costello, G. O'Sullivan, M. W. D. Mansfield, P. V. Demekhin, B. M. Lagutin, and V. L. Sukhorukov, Phys. Rev. A **67**, 042707 (2003).

[50] J. M. Bizau, C. Blancard, M. Coreno, D. Cubaynes, C. Dehon, N. El Hassan, F. Folkmann, M. F. Gharaibeh, A. Giuliani, J. Lemaire, A. R. Milosavljević, C. Nicolas, and R. Thissen, J. Phys. B: At. Mol. Opt. Phys. **44**, 055205 (2011).

[51] G. Hinojosa, A. M. Covington, G. A. Alna'Washi, M. Lu, R. A. Phaneuf, M. M. Sant'Anna, C. Cisneros, I. Álvarez, A. Aguilar, A. L. D. Kilcoyne, A. S. Schlachter, C. P. Ballance, and B. M. McLaughlin, Phys. Rev. A **86**, 063402 (2012).

[52] D. L. Miller, J. D. Dow, R. G. Houlgate, G. V. Marr, and J. B. West, J. Phys. B: At. Mol. Phys. **10**, 3205 (1977).

[53] P. V. Demekhin, I. D. Petrov, B. M. Lagutin, V. L. Sukhorukov, F. Vollweiler, S. Klumpp, A. Ehresmann, K.-H. Schartner, and H. Schmoranzer, J. Phys. B: At. Mol. Opt. Phys. **38**, 3129 (2005).

[54] E. Gryzlova, A. Grum-Grzhimailo, E. Staroselskaya, and S. Strakhova, J. Electron Spectrosc. Relat. Phenom. **204**, 277 (2015).

[55] U. Fano and J. W. Cooper, Phys. Rev. **137**, A1364 (1965).